Mass-polariton theory of sharing the total angular momentum of light between the field and matter

Mikko Partanen and Jukka Tulkki
Engineered Nanosystems group, School of Science, Aalto University, P.O. Box 11000, 00076 Aalto, Finland

(Received 13 April 2018; published 11 September 2018)

Light propagating in a nondispersive medium is accompanied by a mass density wave (MDW) of atoms set in motion by the optical force of the field itself [Phys. Rev. A **95**, 063850 (2017)]. This recent result is in strong contrast with the approximation of fixed atoms, which assumes that atoms are fixed to their equilibrium positions when light propagates in a medium and which is deeply rooted in the conventional electrodynamics of continuous media. In many photonic materials, the atoms carry the majority of the total momentum of light and their motion also gives rise to net transfer of medium mass with a light pulse. In this work we use optoelastic continuum dynamics combining the optical force field, elasticity theory, and Newtonian mechanics to analyze the angular momentum carried by the MDW. Our calculations are based on classical physics, but by dividing the numerically calculated angular momenta of Laguerre-Gaussian (LG) pulses with the photon number, we can also study the single-quantum values. We show that accounting for the MDW in the analysis of the angular momentum gives for the field's share of the total angular momentum of light a quantized value that is generally a fraction of $\hbar$. In contrast, the total angular momentum of the mass-polariton (MP) quasiparticle, which is a coupled state of the field and the MDW, and also the elementary quantum of light in a medium, is an integer multiple of $\hbar$. Thus, the angular momentum of the MP has coupled field and medium components, which cannot be separately experimentally measured. This discovery is related to the previous observation that a bare photon including only the field part cannot propagate in a medium. The same coupling is found for orbital and spin angular momentum components. The physical picture of the angular momentum of light emerging from our theory is fundamentally more general than earlier theoretical models, in which the total angular momentum of light is assumed to be carried by the electromagnetic field only or by an electronic polariton state, which also involves dipolar electronic oscillations. These models cannot describe the MDW shift of atoms associated with light. We simulate the MDW of LG pulses in silicon and present a schematic experimental setup for measuring the contribution of the atomic MDW to the total angular momentum of light.

DOI: 10.1103/PhysRevA.98.033813

I. INTRODUCTION

Since the pioneering theoretical work of Allen *et al.* [1], there has been rapid progress in both theoretical and experimental studies of the angular momentum of light [2–18]. In the groundbreaking works, the angular momentum of light has been split into orbital angular momentum (OAM) and spin angular momentum (SAM) [19–21]. The OAM is related to the helical phasefronts of optical vortex beams and it is described by the vortex topological charge $l \in \{0, \pm 1, \pm 2, \dots\}$, and the SAM is related to the circular polarization of the wave and it is described by the polarization helicity $\sigma \in [-1, 1]$ [22,23].

The photon angular momentum has been considered both in vacuum and in various photonic materials also in the near-field regime [24–26]. Advances have been made also in the understanding of the topological and phase properties of light [22,27–33]. Interestingly, the recently developed mass-polariton (MP) theory of light [34,35] shows that, in many photonic materials, the majority of the momentum of light is carried by the medium atoms. This theory questions the conventional approximation of fixed atomic positions in the description of propagation of light in a medium. Thus, a question arises: what happens in a nondispersive dielectric when the total angular momentum of light is shared between the electromagnetic field and the medium atoms moving under the influence of the optical force field?

The MP theory of light shows that a light pulse propagating in a medium drives forwards an atomic mass density wave (MDW) [34,35]. The existence of the MDW that propagates with a light pulse follows directly from the classical optoelastic continuum dynamics (OCD), which combines the well-known optical force density and the elasticity theory with the Newtonian dynamics of the medium. In the single-photon picture, the coupling of the electromagnetic field to the atomic MDW gives rise to MP quasiparticles, which are covariant coupled states of the field and matter.

The MP quasiparticles carry a total momentum of the Minkowski form $p_{\mathrm{MP}} = n\hbar\omega/c$, where n is the refractive index of the nondispersive medium, $\hbar$ is the reduced Planck constant, ω is the angular frequency, and c is the speed of light in vacuum [35]. The total MP momentum is split between the electromagnetic field and the MDW so that the share of the field corresponds to the Abraham momentum $p_{\mathrm{field}} = \hbar\omega/(nc)$ and the MDW carries the difference of the Minkowski and Abraham momenta $p_{\mathrm{MDW}} = p_{\mathrm{MP}} - p_{\mathrm{field}}$.

In this work we show that the MP theory of light can and must be used to describe the angular momentum of light in nondispersive media. We will also show that sharing of the angular momentum between the field and matter is related to fundamental quantum properties of light. A single quantum of circularly polarized light is well known to carry an angular

momentum $\hbar$. Here we will show that, e.g., in the case of silicon and assuming a wavelength of $\lambda_0 = 1550$ nm, it is shared between the field ($0.083\hbar$) and the MDW ($0.917\hbar$). Since both these partial angular momenta are fractions of $\hbar$, also a fundamental question arises regarding the quantization of light in a medium. Our results strongly suggest that only the quantum of the coupled state of the electromagnetic field and the medium has a real physical meaning. We also present a schematic experimental setup for the measurement of the azimuthal atomic displacements related to the angular momentum transfer of the MDW in optical fibers.

This work is organized as follows: Section II describes the theoretical foundations of the description of angular momentum in the MP theory of light. Section III presents the Laguerre-Gaussian (LG) mode pulses that are known to carry angular momentum. The OCD simulations of the propagation of selected LG mode light pulses in a medium are presented in Sec. IV. In Sec. VI we discuss whether the atomic MDW has an effect in the analysis of previous microparticle rotation experiments [11–14,36–38]. A schematic plan of the fiber rotation experiment for the experimental verification of the azimuthal atomic displacement of the MDW is presented in Sec. VII. Finally, conclusions are drawn in Sec. VIII.

II. ANGULAR MOMENTUM IN THE MASS-POLARITON THEORY

A. Angular momentum of the electromagnetic field

The fundamental expression of the total angular momentum of the electromagnetic field in vacuum is conventionally given by [20,21,39–59]

$$\mathbf{J}_{\text{field}} = \int \mathbf{r} \times \left(\frac{\mathbf{E} \times \mathbf{H}}{c^2} \right) d^3 r, \tag{1}$$

where $\mathbf{E} \times \mathbf{H}/c^2 = \mathbf{g}_{\text{field}}$ is the linear momentum density of the electromagnetic field [39,40], N_{ph} is the photon number, and $\hat{\mathbf{z}}$ is the unit vector in the direction of propagation. In the MP theory of light, Eq. (1) describes only the electromagnetic field's share of the total angular momentum of light. This result is independent of the conventional separation of the angular momentum of the electromagnetic field into SAM and OAM and into the external and internal parts, which are briefly discussed in Appendix A.

Note that, in previous works neglecting the atomic MDW [25,60], the correct total angular momentum of light in a medium has been obtained by assuming the Minkowski angular momentum density $\mathbf{r} \times (\mathbf{D} \times \mathbf{B})$ for the field. The assumption that the Minkowski angular momentum density is carried by the pure electromagnetic field or by the electronic polariton state involving oscillations of electrons around fixed nuclei cannot explain the MDW associated with light in a medium as described by the MP theory of light [34,35].

B. Beyond the approximation of fixed atoms

The approximation of fixed atoms is conventionally used in the electrodynamics of continuous media [39,40]. In this approximation the atomic nuclei are fixed to their equilibrium positions and they respond to the electromagnetic field only through polarization. Conventionally, the atoms have been assumed to be bound to their positions (or relative positions in the case of moving media) as their total mass energy is extremely large compared to the energy scale of optical fields. Consequently, during the short interaction time of the medium atoms and the propagating optical field, the optical force can move atoms only by an exceedingly small amount. Traditionally, this small atomic movement has been considered to be totally negligible.

This approximation would be justified if the polariton state of light would include only electronic oscillations as is conventionally assumed, for instance, in the case of exciton polaritons and in the simple Lorentz oscillator model of dielectric permittivity. If we only account for the electronic polariton state, the center of masses of the negative electron density and the positive nucleon density move in opposite directions and the total center of mass of the atom stands still. Both these mass shifts are anyway, for a free plane-wave field in a nondispersive medium, considered to be parallel to the electric field vector, i.e., orthogonal to the wave vector, and thus cannot contribute to the MDW, which propagates in the direction of the Poynting vector.

Recently, the approximation of fixed atoms has been questioned by the results of the MP theory of light and the related computer simulations based on the OCD model [34,35]. Coupling the conventional electrodynamics and elasticity theories of continuous media, the OCD model shows that the collective small motion of atoms forms an atomic MDW. Since coupled systems have been under detailed studies in many fields of physics for decades, it is surprising that the coupled dynamics of the electromagnetic field and the atomic MDW has not been studied in detail already much earlier.

We note here an early paper by Poynting [61], where the existence of "small longitudinal material waves accompanying light waves" is foretold. Thus, he considered essentially the same phenomenon as the MDWs in the MP theory of light. Poynting made his calculations in the most simple case of an electromagnetic plane wave. He also correctly calculated the very small kinetic energy associated to the MDWs. However, he did not calculate the mass energy, which is transferred with these waves. Therefore, the relation of these waves to the covariance principle of the special theory of relativity and to the conservation of the center of energy velocity of an isolated system was not recovered. In addition, he did not study whether these waves could carry angular momentum.

C. Newton's equation of motion

In the OCD model, the coupling between the field and matter is described by Newton's equation of motion. As the atomic velocities are nonrelativistic, Newton's equation of motion for the mass density of the medium $\rho_{\text{a}}(\mathbf{r}, t)$ is given by

$$\rho_{\text{a}}(\mathbf{r}, t) \frac{d^2 \mathbf{r}_{\text{a}}(\mathbf{r}, t)}{dt^2} = \mathbf{f}_{\text{opt}}(\mathbf{r}, t) + \mathbf{f}_{\text{el}}(\mathbf{r}, t), \tag{2}$$

where $\mathbf{r}_{\text{a}}(\mathbf{r}, t)$ is the position- and time-dependent atomic displacement field of the medium, $\mathbf{f}_{\text{opt}}(\mathbf{r}, t)$ is the optical force density experienced by atoms, given in Eq. (3) below, and $\mathbf{f}_{\text{el}}(\mathbf{r}, t)$ is the elastic force density between atoms that are displaced from their initial equilibrium positions by the

optical force density. The elastic force density for anisotropic cubic crystals, such as silicon, is given, e.g., in Ref. [62].

For the optical force density, we use the expression that is well known in previous literature [39,40]. It is given for a dielectric medium by [63]

$$\mathbf{f}_{\rm opt}(\mathbf{r},t) = -\frac{\varepsilon_0}{2}\mathbf{E}^2\nabla n^2 + \frac{n^2-1}{c^2}\frac{\partial}{\partial t}\mathbf{E}\times\mathbf{H}. \tag{3}$$

Note that the OCD model enables the use of any physically meaningful form of the optical force density in solving the dynamical equations [63]. However, the different terms cannot be arbitrarily modified without breaking the momentum conservation and the relativistic covariance condition [34,35].

The optical force density in Eq. (3) leads to the transfer of a part of the total momentum of light by the MDW [34,35]. In this work we show that the optical force density in Eq. (3) is also responsible for the description of the optical torque in the medium and the related transfer of a substantial part of the total angular momentum of light by the MDW. In calculating the optoelastic force field, we have neglected the extremely small damping of the electromagnetic field due to the transfer of field energy to the kinetic and elastic energies of the medium. The accuracy of this approximation is estimated in Ref. [34].

D. Angular momentum of the mass density wave

The angular momentum density of the MDW can be written according to classical mechanics as

$$\mathbf{J}_{\rm MDW} = \int \mathbf{r}\times\rho_{\rm a}\mathbf{v}_{\rm a}d^3r, \tag{4}$$

where $\rho_{\rm a}\mathbf{v}_{\rm a} = \mathbf{g}_{\rm MDW}$ is the linear momentum density of the MDW [34]. This classical angular momentum of the MDW follows purely from the motion of atoms in the MDW driven by the optical force density. Whether there exist any experimentally feasible ways to separate this total angular momentum of the MDW into OAM and SAM parts will be discussed below and is partly left as a topic of further work.

The total angular momentum of the coupled MP state of the field and matter is given by the sum of the field and MDW contributions as

$$\mathbf{J}_{\rm MP} = \int \mathbf{r}\times\left(\rho_{\rm a}\mathbf{v}_{\rm a} + \frac{\mathbf{E}\times\mathbf{H}}{c^2}\right)d^3r, \tag{5}$$

where $\rho_{\rm a}\mathbf{v}_{\rm a} + \mathbf{E}\times\mathbf{H}/c^2 = \mathbf{g}_{\rm MP}$ is the total linear momentum density of the MP. As shown by the computer simulations below, the angular momentum of the MDW is an integral part of the total angular momentum of light in a medium.

III. FIELDS CARRYING ANGULAR MOMENTUM

A. Laguerre-Gaussian pulses

It is well known that helically phased light carries OAM regardless of the radial distribution of the fields [19]. However, it is often useful to express beams in a complete basis set of orthogonal modes. A convenient choice as the basis set for beams that carry OAM is provided by the LG modes.

The LG mode function for the mode LG_{pl} is given in the limit of constant beam waist or large Rayleigh range as [1,64]

$$u_{p,l}(r,\phi) = u_0\left(\frac{\sqrt{2}r}{w_0}\right)^{|l|}e^{-r^2/w_0^2}e^{il\phi}L_p^{|l|}\left(\frac{2r^2}{w_0^2}\right), \tag{6}$$

where L_p^l are the generalized Laguerre polynomials, u_0 is a normalization constant that also depends on the values of p and l, and w_0 is the waist radius [1]. The waist radius is a distance where the intensity of the beam has dropped to $1/e^2$ of its on-axis value.

B. Linear polarization

The electric and magnetic fields of a LG beam with linear polarization along the x direction are written in the paraxial approximation for a given wave number k as presented, e.g., in Refs. [1,65,66]. Here we study a light pulse with a Gaussian distribution for k as described by the Gaussian function $u(k) = e^{-[(k-nk_0)/(n\Delta k_0)]^2/2}/(\sqrt{2\pi}\,n\Delta k_0)$, where $k_0 = \omega_0/c$ is the wave number in vacuum for central frequency ω_0, and Δk_0 is the standard deviation of the wave number in vacuum. Therefore we write the electric and magnetic fields of the LG_{pl} pulse as

$$\mathbf{E}_{p,l}(\mathbf{r},t) = \mathrm{Re}\left[\int_{-\infty}^{\infty} i\omega(k)\left(u_{p,l}\hat{\mathbf{x}} + \frac{i\partial u_{p,l}}{k\partial x}\hat{\mathbf{z}}\right)u(k)e^{i[kz-\omega(k)t]}dk\right], \tag{7}$$

$$\mathbf{H}_{p,l}(\mathbf{r},t) = \mathrm{Re}\left[\int_{-\infty}^{\infty} \frac{ik}{\mu_0}\left(u_{p,l}\hat{\mathbf{y}} + \frac{i\partial u_{p,l}}{k\partial y}\hat{\mathbf{z}}\right)u(k)e^{i[kz-\omega(k)t]}dk\right], \tag{8}$$

where $\omega(k) = ck/n$ is the dispersion relation of a nondispersive medium.

The wave number and its standard deviation in the medium are given in terms of the vacuum quantities by $k_{0,\rm med} = nk_0$ and $\Delta k_{0,\rm med} = n\Delta k_0$. The standard deviations of the x and y components of the wave number are given by $\Delta k_x = \Delta k_y = \sqrt{2}/w_0$. The standard deviations of the spatial dimensions of the pulse energy density are $\Delta z = 1/(\sqrt{2}\Delta k_{0,\rm med})$ and $\Delta x = \Delta y = 1/(\sqrt{2}\Delta k_x) = w_0/2$. The corresponding standard deviation in time is then $\Delta t = n\Delta z/c = 1/(\sqrt{2}\Delta k_0 c)$ and the full width at half maximum is $\Delta t_{\rm FWHM} = 2\sqrt{2\ln 2}\Delta t$.

In the monochromatic field limit, the fields in Eqs. (7) and (8) and the resulting Poynting vector can be approximated further as explained in Appendix B. This approximation allows us to perform the integrations in Eqs. (7) and (8) analytically, which reduces the computational power needed in the three-dimensional simulations. As shown in Ref. [34], we can also approximate the actual instantaneous Poynting vector of a light pulse with its time average over the harmonic cycle without losing accuracy in the calculation of the total quantities, such as the linear and angular momenta and the transferred mass of the light pulse.

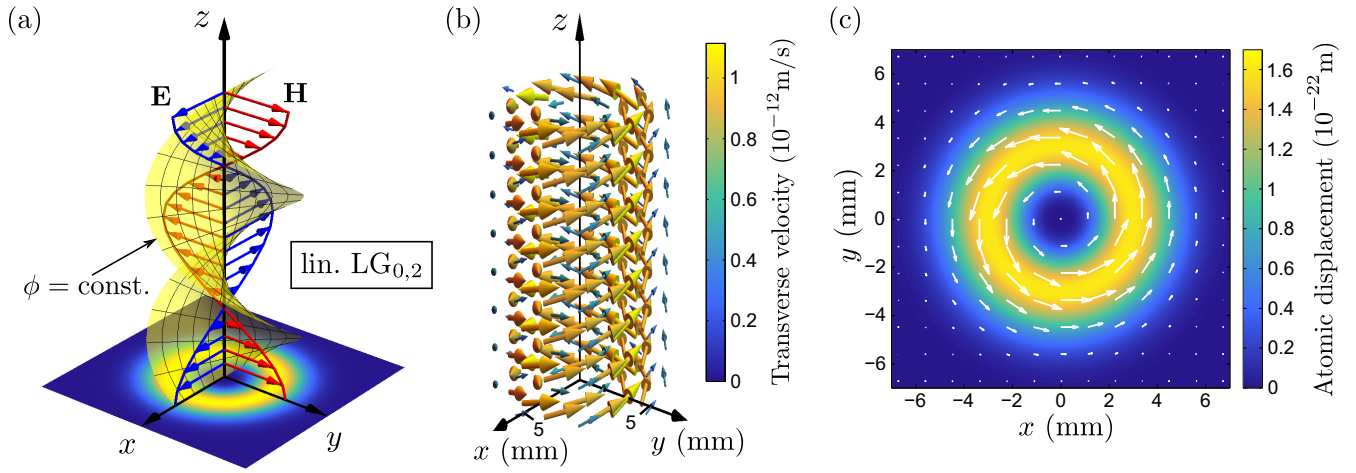

FIG. 1. Simulations for a linearly polarized $LG_{0,2}$ pulse that carries OAM in silicon. (a) The electric field polarization lies in the vertical plane $y = 0$ as the polarization is linear. The opaque surface shows the helical phasefront of the pulse. The density plot in the plane $z = 0$ shows the time-averaged field intensity. (b) The vector arrows present the time-averaged atomic velocities in the MDW driven by the field. In the z direction, the plot region corresponds to one harmonic cycle in the middle of the pulse. The z component of the atomic velocities dominates and it has been scaled down using a factor of 10^{-5} to make the spiraling of the atomic velocities around the optical axis visible. The colors correspond to the magnitude of the transverse component of the atomic velocities. (c) Representation of the azimuthal atomic displacement due to the transfer of OAM with the MDW of atoms. The vector arrows show the direction and the color bar shows the magnitude. The atomic displacement is represented at the instance of time just after the pulse has gone and elastic forces have not had enough time to relax the strain field related to these atomic displacements.

C. Circular polarization

As defined from the point of view of the source, the electric and magnetic fields of a right circularly polarized LG_{pl} pulse are given in the paraxial approximation by [65,67]

$$\mathbf{E}_{p,l}(\mathbf{r},t) = \frac{1}{\sqrt{2}}\mathrm{Re}\left[\int_{-\infty}^{\infty} i\omega(k)\left(u_{p,l}\hat{\mathbf{x}} + \frac{i\partial u_{p,l}}{k\partial x}\hat{\mathbf{z}}\right)u(k)e^{i[kz-\omega(k)t]}dk + \int_{-\infty}^{\infty} i\omega(k)\left(u_{p,l}\hat{\mathbf{y}} + \frac{i\partial u_{p,l}}{k\partial y}\hat{\mathbf{z}}\right)u(k)e^{i[kz-\omega(k)t+\pi/2]}dk\right], \tag{9}$$

$$\mathbf{H}_{p,l}(\mathbf{r},t) = \frac{1}{\sqrt{2}}\mathrm{Re}\left[\int_{-\infty}^{\infty} \frac{ik}{\mu_0}\left(u_{p,l}\hat{\mathbf{y}} + \frac{i\partial u_{p,l}}{k\partial y}\hat{\mathbf{z}}\right)u(k)e^{i[kz-\omega(k)t]}dk - \int_{-\infty}^{\infty} \frac{ik}{\mu_0}\left(u_{p,l}\hat{\mathbf{x}} + \frac{i\partial u_{p,l}}{k\partial x}\hat{\mathbf{z}}\right)u(k)e^{i[kz-\omega(k)t+\pi/2]}dk\right]. \tag{10}$$

These fields can be seen as superpositions of two linearly polarized fields, whose transverse components are orthogonal to each other, and which have a phase difference of $\pi/2$. The first terms in Eqs. (9) and (10) correspond to the linearly polarized fields in Eqs. (7) and (8).

As in the case of linear polarization above, in the monochromatic field limit, the fields in Eqs. (9) and (10) and the resulting Poynting vector can be approximated further as explained in Appendix B.

IV. ANGULAR MOMENTUM SIMULATIONS

Next we simulate the propagation of LG light pulses in silicon. We simulate a pulse, which has a total electromagnetic energy of $U_0 = 5$ mJ and a central vacuum wavelength of $\lambda_0 = 1550$ nm. These values correspond to the central angular frequency of $\omega_0 = 2\pi c/\lambda_0 = 1.215 \times 10^{15}\,\mathrm{s}^{-1}$ and the photon number of $N_{\mathrm{ph}} = U_0/\hbar\omega_0 = 3.901 \times 10^{16}$. The phase and group refractive indices of silicon are given by $n_{\mathrm{p}} = 3.4757$ and $n_{\mathrm{g}} = 3.5997$ for $\lambda_0 = 1550$ nm [68]. Since the dispersion is not very large, for simplicity, in this work we neglect the dispersion and use the phase refractive index only. However, the dispersion could be accounted for in the MP theory of light as shown in Ref. [34].

The lateral width of the LG mode in Eq. (6) is determined by $\Delta k_x = \Delta k_y = \sqrt{2}/w_0 = 10^{-4}k_0$, which correspond to the waist radius of $w_0 \approx 3.5$ mm. The longitudinal pulse width is determined by the spectral width $\Delta\omega/\omega_0 = \Delta k_0/k_0 = 10^{-5}$, which corresponds to $\Delta z \approx 5.0$ mm and $\Delta t_{\mathrm{FWHM}} \approx 140$ ps. The normalization constant u_0 in Eq. (6) becomes fixed by requiring that the total electromagnetic energy of the pulse is U_0 as defined above.

In the simulations we also use the mass density of silicon, which is $\rho_0 = 2329\,\mathrm{kg/m}^3$ [69], and the elastic constants in the direction of the (100) plane, which are $C_{11} = 165.7$ GPa, $C_{12} = 63.9$ GPa, and $C_{44} = 79.6$ GPa [70]. These elastic constants correspond to the bulk modulus of $B = (C_{11} + 2C_{12})/3 = 97.8$ GPa and the shear modulus of $G = C_{44} = 79.6$ GPa.

A. Simulations for orbital angular momentum

First, we consider the OAM related to the MDW of moving atoms. As an example, we use a linearly polarized $LG_{0,2}$ pulse that is well known to carry OAM as $l = 2$. The SAM of this pulse is zero due to linear polarization for which $\sigma = 0$.

Figure 1(a) illustrates the linearly polarized $LG_{0,2}$ mode. The vector arrows in Fig. 1(a) present the directions of the instantaneous electric (blue) and magnetic (red) fields. For

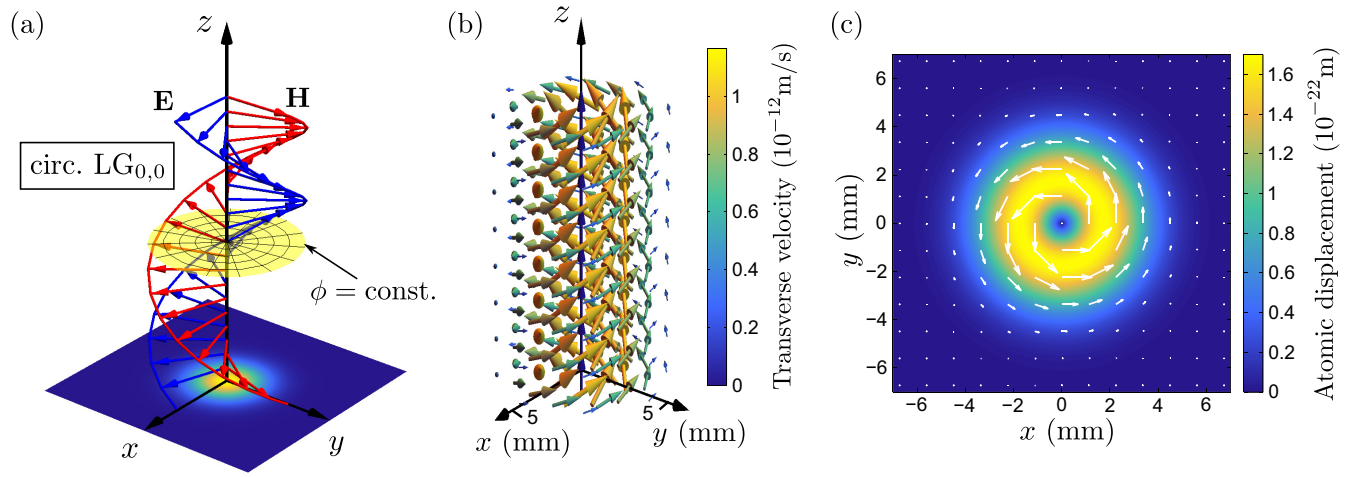

FIG. 2. Simulations for a right circularly polarized $LG_{0,0}$ pulse that carries SAM in silicon. (a) The position dependence of the transverse component of the electric field polarization forms a helical surface as the polarization is circular. The opaque surface shows the plane of constant phase. The density plot in the plane $z = 0$ shows the time-averaged field intensity. (b) The vector arrows present the time-averaged atomic velocities in the MDW driven by the field. In the z direction, the plot region corresponds to one harmonic cycle in the middle of the pulse. The z component of the atomic velocities dominates and it has been scaled down using a factor of 10^{-5} to make the spiraling of the atomic velocities around the optical axis visible. The colors correspond to the magnitude of the transverse component of the atomic velocities. (c) Representation of the azimuthal atomic displacement due to the transfer of OAM with the MDW of atoms. The vector arrows show the direction and the color bar shows the magnitude. The atomic displacement is represented at the instance of time just after the pulse has gone and elastic forces have not had enough time to relax the strain field related to these atomic displacements.

our linearly polarized field, the electric field vectors lie in the plane $y = 0$ while the magnetic field vectors are located in the plane $x = 0$. The exact spatial distributions of the fields are, however, more complex and not shown in the figure. The opaque surface shows the phasefront of the pulse, which forms a double helix for our pulse with $l = 2$. The density plot in the plane $z = 0$ shows the time-averaged field intensity. The field intensity has a vortex at $x = y = 0$, which is characteristic for all higher order LG modes.

Figure 1(b) shows the time-averaged atomic velocities in the MDW driven by a linearly polarized $LG_{0,2}$ pulse. The z component of the atomic velocities dominates and it has been scaled down using a factor of 10^{-5} to make the transverse velocity components visible. The atomic velocities are seen to spiral around the optical axis so that the velocity distribution of atoms has a vortex at $x = y = 0$. The velocity distribution of atoms in the MDW clearly follows the field intensity in the density plot in Fig. 1(a). This is an expected result since the optical force density in the second term of Eq. (3) driving the atomic MDW forwards is determined by the Poynting vector.

The atomic velocity distribution of the light pulse obtained in the simulations can be used with Eq. (4) to calculate the angular momentum of the MDW. Within the numerical accuracy of the simulations and the monochromatic field approximation described in Appendix B, we obtain $\mathbf{J}_{\mathrm{MDW}} = 7.157 \times 10^{16}\hbar\hat{\mathbf{z}}$. For the angular momentum of the electromagnetic field, given by Eq. (1), we obtain $\mathbf{J}_{\mathrm{field}} = 6.459 \times 10^{15}\hbar\hat{\mathbf{z}}$. Dividing these values with the photon number of the pulse gives $\mathbf{J}_{\mathrm{MDW}}/N_{\mathrm{ph}} = 1.834\hbar\hat{\mathbf{z}}$ and $\mathbf{J}_{\mathrm{field}}/N_{\mathrm{ph}} = 0.166\hbar\hat{\mathbf{z}}$. The sum of these angular momenta is the total angular momentum of the mass polariton, given by $\mathbf{J}_{\mathrm{MP}}/N_{\mathrm{ph}} = 2\hbar\hat{\mathbf{z}}$. This equals the expected total angular momentum of the linearly polarized $LG_{0,2}$ mode with $l = 2$ and $\sigma = 0$. Therefore, our results indicate that the total angular momentum of light in a medium is split between the field and the MDW in such a way that the MDW carries a substantial part of the total angular momentum of light.

Figure 1(c) shows the transverse component of the simulated atomic displacement for the linearly polarized $LG_{0,2}$ pulse just after the light pulse has gone. The time-dependent simulations of the atomic displacements and velocities in a fixed transverse plane are presented as a video file in the Supplemental Material [71]. In the passage of the pulse, the atomic displacements monotonically increase to their maximum values, whose transverse components are shown in Fig. 1(c). In contrast, the average atomic velocity increases in the pulse front, obtains its maximum value in the middle of the pulse, and decreases to zero in the tail of the pulse.

B. Simulations for spin angular momentum

Next, we consider the SAM of the atomic MDW by simulating the propagation of a right circularly polarized $LG_{0,0}$ pulse. This pulse carries SAM but no OAM as $l = 0$ and $\sigma = 1$.

Figure 2(a) illustrates the right circularly polarized $LG_{0,0}$ mode. The vector arrows show the directions of the instantaneous electric (blue) and magnetic (red) fields. These field vectors form polarization surfaces that are helical for our circularly polarized field. The opaque surface shows the phasefront of the pulse. In contrast to the higher order $LG_{0,2}$ pulse in Fig. 1(a), the phasefront is a plane for our $LG_{0,0}$ pulse with $l = 0$. The density plot in the transverse plane $z = 0$ shows the cross section of the time-averaged field intensity. In contrast to the case of the $LG_{0,2}$ pulse in Fig. 1(a), the field intensity in Fig. 2(a) obtains its maximum value at $x = y = 0$

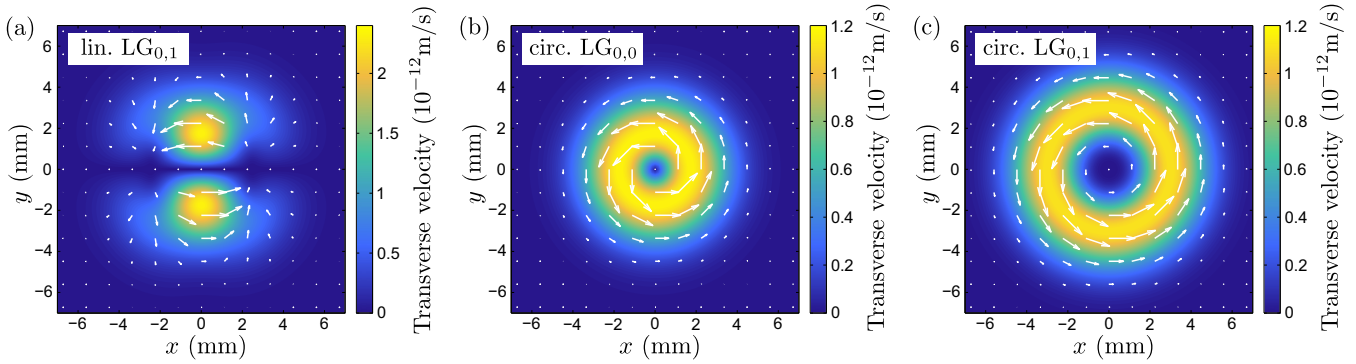

FIG. 3. Instantaneous atomic velocity in the MDW. The position dependence of the transverse component of the instantaneous atomic velocity of the MDW (a) for the linearly polarized $LG_{0,1}$ pulse carrying OAM of $N_{\rm ph}\hbar$, (b) for the circularly polarized $LG_{0,0}$ pulse carrying SAM of $N_{\rm ph}\hbar$, and (c) for the circularly polarized $LG_{0,1}$ pulse carrying both OAM of $N_{\rm ph}\hbar$ and SAM of $N_{\rm ph}\hbar$. The transverse atomic velocities are plotted for one instance of time in the middle of the pulse.

for the $LG_{0,0}$ pulse. Therefore, there is not any vortex in the field intensity when $l = 0$.

Figure 2(b) shows the time-averaged atomic velocities in the MDW driven by the right circularly polarized $LG_{0,0}$ pulse. The atomic velocities are again seen to spiral around the direction of propagation along the z axis. Again, the z component of the atomic velocities dominates and it has been scaled down using a factor of 10^{-5} to make the transverse velocity components visible. Whereas in Fig. 1 the spiraling of the atomic velocities followed from the higher order nature of the $LG_{0,2}$ pulse, here the spiraling follows purely from the circular polarization. As in the case of OAM in Fig. 1, the atomic velocities in the MDW driven by the circularly polarized light pulse carrying only SAM also follow the field intensity in the density plot in Fig. 2(a). Again, this follows from the fact that the optical force density in the second term of Eq. (3) driving the atomic MDW forwards is determined by the Poynting vector.

Using Eq. (4) and the atomic velocity distribution of the MDW obtained in the simulations, we can again calculate the angular momentum of the MDW. Within the monochromatic field approximation described in Appendix B and the numerical accuracy of the simulations, we obtain $\mathbf{J}_{\rm MDW} = 3.578 \times 10^{16}\hbar\hat{\mathbf{z}}$. The corresponding angular momentum of the electromagnetic field, given by Eq. (1), has a value of $\mathbf{J}_{\rm field} = 3.230 \times 10^{15}\hbar\hat{\mathbf{z}}$. Dividing the angular momenta of the MDW and the electromagnetic field with the photon number of the pulse gives $\mathbf{J}_{\rm MDW}/N_{\rm ph} = 0.917\hbar\hat{\mathbf{z}}$ and $\mathbf{J}_{\rm field}/N_{\rm ph} = 0.083\hbar\hat{\mathbf{z}}$. Summing these angular momenta together then gives total angular momentum of the mass polariton as $\mathbf{J}_{\rm MP}/N_{\rm ph} = \hbar\hat{\mathbf{z}}$, which is an expected result for the right circularly polarized $LG_{0,0}$ mode with $l = 0$ and $\sigma = 1$. Therefore, these results give further support for the splitting of the total angular momentum of light between the field and the MDW.

Figure 2(c) shows the transverse component of the simulated atomic displacement for the right circularly polarized $LG_{0,0}$ pulse just after the light pulse has gone. The time-dependent simulations of the atomic displacements and velocities in a fixed transverse plane are presented as a video file in the Supplemental Material [71]. In the passage of the pulse, the atomic displacements again monotonically increase to their maximum values, while the average atomic velocity increases in the pulse front, obtains its maximum value in the middle of the pulse, and decreases to zero in the tail of the pulse.

C. Differences in the instantaneous mass density waves

Figure 3 shows the transverse components of the instantaneous atomic velocities in the MDWs of the linearly polarized $LG_{0,1}$ pulse carrying OAM ($N_{\rm ph}\hbar$), the circularly polarized $LG_{0,0}$ pulse carrying SAM ($N_{\rm ph}\hbar$), and the circularly polarized $LG_{0,1}$ pulse carrying both OAM ($N_{\rm ph}\hbar$) and SAM ($N_{\rm ph}\hbar$). One can directly observe the notable difference that, in the case of linear polarization in Fig. 3(a) (see also a video file in the Supplemental Material [71]), the atomic velocities vary as a function of the azimuthal angle, whereas in the case of circular polarizations in Figs. 3(b) and 3(c), this azimuthal dependence is missing. Therefore, we can conclude that the MDW component that has azimuthal variations is related to the linear polarization while the MDW component that is approximately constant in the azimuthal direction is related to the circular polarization. Thus, the MDWs of linearly and circularly polarized light pulses are in principle separable. However, whether the physical separation into the OAM and SAM components is possible in the general case of a pulse carrying both OAM and SAM remains an open question in the classical regime where one can in principle measure the transverse velocity distribution and the shift of atoms in the MDW. However, for a single light quantum in a medium, our results strongly suggest that the total angular momentum of the quantum, which is an integer multiple of $\hbar$, cannot be divided in a physically meaningful way into the OAM and SAM components of either the MDW or the electromagnetic field.

V. COMPARISON OF THE OCD AND MP QUASIPARTICLE MODEL RESULTS

For a general Laguerre-Gaussian pulse with total electromagnetic energy $U_0 = N_{\rm ph}\hbar\omega_0$, we can calculate the numerical values of the angular momenta in Eqs. (1), (4), and (5). Within the numerical accuracy of the simulations,

we obtain

$$\mathbf{J}_{\text{field}} = \int \mathbf{r} \times \left(\frac{\mathbf{E} \times \mathbf{H}}{c^2} \right) d^3r = (l+\sigma) \frac{N_{\text{ph}} \hbar}{n^2} \hat{\mathbf{z}}, \quad (11)$$

$$\mathbf{J}_{\text{MDW}} = \int \mathbf{r} \times \rho_{\text{a}} \mathbf{v}_{\text{a}} d^3r = \left(1 - \frac{1}{n^2} \right) (l+\sigma) N_{\text{ph}} \hbar \hat{\mathbf{z}}, \quad (12)$$

$$\mathbf{J}_{\text{MP}} = \int \mathbf{r} \times \left(\rho_{\text{a}} \mathbf{v}_{\text{a}} + \frac{\mathbf{E} \times \mathbf{H}}{c^2} \right) d^3r = (l+\sigma) N_{\text{ph}} \hbar \hat{\mathbf{z}}, \quad (13)$$

i.e., the numerically calculated values of the integrals are equal to the right-hand side results within seven digits. Thus, the right-hand side results divided by the photon number represent the single quantum MP quasiparticle model values of the corresponding angular momenta.

Equations (11)–(13) indicate that the total angular momentum of light in a nondispersive medium is split between the field and the MDW in the same ratio $\mathbf{J}_{\text{MDW}}/\mathbf{J}_{\text{field}} = n^2 - 1$ as the total linear momentum $p_{\text{MDW}}/p_{\text{field}}$ and energy $E_{\text{MDW}}/E_{\text{field}}$ shown in Refs. [34,35]. The comparison of Eqs. (11)–(13) shows that the atomic MDW carries a substantial part (for many photonic materials most) of the total angular momentum of light in a medium. In previous works on the angular momentum of light in a medium [25,60], which have neglected the atomic MDW, the correct total angular momentum of light has been obtained by assuming that the field carries the Minkowski momentum, which corresponds to the angular momentum density $\mathbf{r} \times (\mathbf{D} \times \mathbf{B})$. According to the MP theory of light, this assumption is not justified [34,35].

VI. ANALYZING MICROPARTICLE ROTATION EXPERIMENTS

It is worth to consider whether the MDW has an effect in the previous microparticle rotation experiments performed to probe the OAM and SAM of light [11–14,36–38]. These experiments are based on trapping particles by using optical tweezers, which rely on the gradient force to confine a dielectric particle near the point of highest light intensity [13,72]. It has been observed that the OAM and SAM of light result in the rotation of absorptive [11,36,37] and birefringent [12–14] particles. Therefore, the physical mechanism of the observed angular momentum transfer is very different compared to the angular momentum of the MDW. In order to observe the angular momentum of the MDW, one should aim at observing the rotation of the homogeneous host medium itself when light propagates through it. This rotation related to the MDW is much smaller than the rotation of a single microparticle and it is not expected to be observable in the previous experiments.

VII. PLANNING OF THE FIBER ROTATION EXPERIMENT

Next, we study how the azimuthal atomic displacement due to the MDW simulated in Sec. IV could be experimentally verified. For this purpose, we propose a fiber rotation experiment, where one measures the rotation of an optical fiber due to optical forces of circularly polarized continuous wave light beams after the fields have been switched on at time $t = 0$ s. These calculations can also inspire experimentalists to design other kinds of setups for the same purpose of verifying the azimuthal atomic displacement predicted by the MP theory

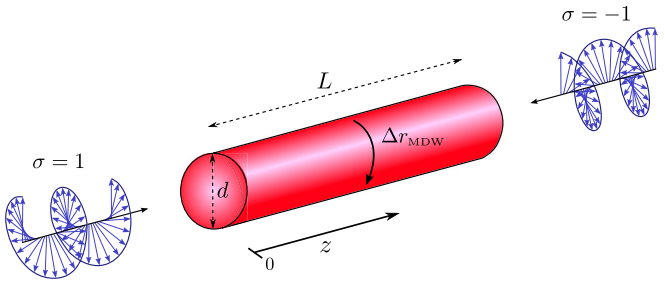

FIG. 4. Schematic experimental setup for measuring the azimuthal rotation displacement Δr_{MDW} of an optical fiber due to the MDWs resulting from the optical forces of circularly polarized continuous wave laser beams. One of the beams has right-handed polarization ($\sigma = 1$) while the polarization of the other beam is left handed ($\sigma = -1$). The rotation is to be measured in the timescale of 0.01 s after the laser beams have been switched on. In longer timescales, the angular momentum transfer due to the optical absorption starts to dominate the MDW effect.

of light. In the relatively long timescale used here, the strain fields in the fiber cross section are assumed to be relaxed by the elastic forces so that all material element in the fiber cross section have approximately the same angle of rotation with respect to the fiber axis. In particular, here we focus on investigating the azimuthal atomic displacement that should be measured at the fiber surface.

A schematic illustration of the proposed setup is presented in Fig. 4. The silicon fiber is expected to rotate due to the optical forces of two circularly polarized light beams propagating in opposite directions. One of the beams has right-handed polarization while the polarization of the other beam is left handed. This way the azimuthal atomic displacements of the MDWs of the two beams add up instead of canceling each other. The fiber and its ends are allowed to rotate freely so that the fiber does not experience external torques. As there are two beams of equal intensities propagating in opposite directions, the total longitudinal atomic displacement in the middle of the fiber, studied in Ref. [35], is approximately zero. In addition to the atomic displacements due to the MDWs, also the optical absorption in the fiber contributes to the total rotation of the fiber. This will be studied below. On the other hand, some secondary effects, such as thermal expansion, cannot significantly influence the rotation of the fiber since they are not azimuthal in nature.

In the following calculations aimed to give order of magnitude estimates, we use the bulk value of the refractive index. In more detailed calculations, it should be replaced with the effective refractive index corresponding to the waveguide design. The waveguide dispersion should also be taken into account. Due to the interface effects, the fiber diameter cannot be directly compared with the fiber diameter of our calculations. The fiber diameter should also be corrected for the possible cladding layer, metallic coating, and other factors that influence the spreading of the pulse energy in the transverse direction. All these factors can be easily accounted for in the OCD simulations. Detailed calculations are presented in a separate work [73].

Using Eq. (4) we obtain that the total angular momentum of the MDW is $J_{\mathrm{MDW}} = (1 - 1/n^2)\sigma U_{\mathrm{in}}/\omega_0$, where U_{in} is the total electromagnetic energy inside the fiber. In terms of the time-averaged intensity I of a single beam in the fiber, one can write $U_{\mathrm{in}} = 2n\pi R^2 L I/c$, where R and L are the radius and length of the cylindrical fiber, respectively. On the other hand, the angular momentum of the MDW can be written as $J_{\mathrm{MDW}} = I_{\mathrm{mi}}\Omega$, where $I_{\mathrm{mi}} = \frac{1}{2}\pi\rho_0 R^4 L$ is the moment of inertia and Ω is the angular velocity of the cylindrical fiber. Setting the two expressions of the angular momentum above as equal gives the angular velocity of the fiber as $\Omega = 4\sigma(n - 1/n)I/(c\,\omega_0\rho_0 R^2)$. The corresponding azimuthal atomic displacement on the surface of the fiber as a function of time is then given by $\Delta r_{\mathrm{MDW}} = R\Omega t = 4\sigma(n - 1/n)It/(c\,\omega_0\rho_0 R)$.

Respectively, one can estimate the azimuthal atomic displacement on the surface of the fiber following from the optical absorption. The total angular momentum absorbed by the fiber in time Δt is given by $\Delta J_{\mathrm{abs}} = (1 - e^{-\alpha L})(2\sigma\pi R^2 I\Delta t/\omega_0) \approx 2\pi\alpha\sigma L R^2 I\Delta t/\omega_0$, where α is the small absorption coefficient of the medium. On the other hand, we have $\Delta J_{\mathrm{abs}} = I_{\mathrm{mi}}\Delta\Omega_{\mathrm{abs}}$. Therefore, the angular acceleration related to the optical absorption is given by $\alpha_{\mathrm{abs}} = \Delta\Omega_{\mathrm{abs}}/\Delta t = 4\alpha\sigma I/(\omega_0\rho_0 R^2)$. The corresponding azimuthal atomic displacement on the surface of the fiber as a function of time is then given by $\Delta r_{\mathrm{abs}} = \frac{1}{2}R\alpha_{\mathrm{abs}}t^2 = 2\alpha\sigma I t^2/(\omega_0\rho_0 R)$.

Above we have derived two contributions to the longitudinal atomic displacement on the surface of the fiber. The effect of the MDW depends linearly on time while the effect of the absorption has a quadratic time dependence. Therefore, the MDW effect dominates at small timescales while the effect of the absorption becomes dominant in the course of time. The timescale at which these effects have equal magnitude can be solved by setting $\Delta r_{\mathrm{MDW}} = \Delta r_{\mathrm{abs}}$, which leads to $t_{\mathrm{eq}} = 2(n - 1/n)/(c\alpha)$. In the case of silicon, absorption is very low at $\lambda_0 = 1550$ nm. The measurements by Schinke *et al.* [74] and Green [75] for $\lambda_0 = 1450$ nm give $\alpha \approx 10^{-8}$ cm^{-1} and the absorption is known to decrease towards $\lambda_0 = 1550$ nm. Therefore, we can conservatively estimate $\alpha = 10^{-8}$ cm^{-1}. This gives $t_{\mathrm{eq}} = 21$ ms.

As shown above, the atomic displacement on the surface of the fiber depends linearly on the field intensity. One must note that the field intensity in the experiment cannot be arbitrarily high. For silicon with $\lambda_0 = 1550$ nm, the bulk value of the breakdown threshold energy density has been reported to be $u_{\mathrm{th}} = 13.3$ J/cm^3 [76], which corresponds to the threshold irradiance of $I_{\mathrm{th}} = u_{\mathrm{th}}c/n = 1.1 \times 10^{11}$ W/cm^2. Using the fiber of diameter $d = 2.5$ μm, assuming $I = \frac{1}{100}I_{\mathrm{th}}$, and setting $t = t_{\mathrm{eq}}$, we obtain $\Delta r_{\mathrm{MDW}} = \Delta r_{\mathrm{abs}} = 2.8$ nm, which corresponds to the total atomic displacement of 5.6 nm. The atomic displacement of this magnitude should be feasible to measure. As the time dependencies of the MDW and absorption contributions are different, one should also be able to distinguish the magnitudes of both effects by observing the change of the atomic displacement as a function of time.

Figure 5 shows the calculated azimuthal atomic displacement Δr_{MDW} on the fiber surface due to the MDW as a function of time and the fiber diameter. As reasoned above, the atomic displacement is largest for small fiber diameters and it has a linear time dependence. In the time range $[0, t_{\mathrm{eq}}]$ shown in the figure, the atomic displacement Δr_{MDW} due to the MDW dominates the atomic displacement Δr_{abs} due to the optical absorption. The contribution Δr_{abs} is not shown in the figure. The simulated nanometer-scale atomic displacements strongly support the experimental feasibility of the measurement of the azimuthal atomic displacement of the MDW.

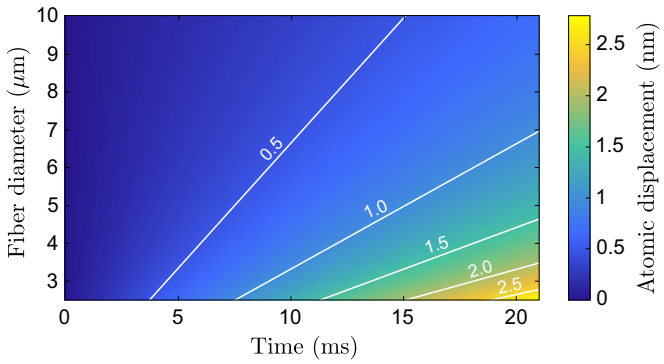

FIG. 5. The calculated total azimuthal atomic displacement due to the MDW on the surface of a cylindrical silicon fiber as a function of time and the fiber diameter. The assumed field intensity is $I = 1.1 \times 10^9$ W/cm^2. The refractive index of silicon for the assumed vacuum wavelength of $\lambda_0 = 1550$ nm is $n = 3.48$. In the time range shown in the figure, the atomic displacement due to the MDW dominates the atomic displacement due to the optical absorption.

It is also important to note that the relatively high intensity, which is needed to produce measurable atomic displacements, can lead to nonlinear effects that must also be accounted for in the implementation of the experiment. To reduce the intensity of single frequency components, one could well use a broad spectrum only requiring that the absorption coefficient is small for the frequencies used. This would allow reducing nonlinear effects, such as the stimulated Brillouin scattering, which is probably the first nonlinear effects that turns on.

VIII. CONCLUSIONS

In conclusion, we have used the MP theory of light to analyze how the angular momentum of light is shared between the field and matter. The optical force density, which gives rise to the momentum of the MDW [34,35], also describes the optical torque. Consequently, in many photonic materials, most of the total angular momentum of light, both OAM and SAM, is not carried by the electromagnetic field but by the MDW. For the electromagnetic field, one obtains a share of the angular momentum that is generally a fraction of $\hbar$. In contrast, the total angular momentum of the MP, where the field is coupled to the MDW, is an integer multiple of $\hbar$. This suggests that the angular momentum of a single quantum in a nondispersive medium has coupled field and medium components. The same coupling is found for OAM and SAM. The coupling that makes it impossible to measure separately the single quantum angular momentum components should not be confused with the well-known quantum entanglement of eigenstates, but it is sooner related to the covariance principle of the special theory of relativity, which prevents a bare photon from existing in a nondispersive medium [34,35]. The generalization of the conventional quantum optical field theory description of light for the presentation of the MDW coupling, studied classically

in the present work, provides an interesting topic for further work.

Our results strongly suggest that a single quantum of light in a nondispersive medium should be understood to include coupled field and medium components. Thus, a single quantum becomes Lorentz invariant and fulfills the constant center of energy law of an isolated system. Compared to earlier theoretical models neglecting the atomic MDW, the physical picture of the angular momentum of light emerging from our theory is fundamentally more general. In previous works, the correct total angular momentum of light in a medium has been obtained only by assuming that the pure electromagnetic field or the electronic polariton state carries the Minkowski momentum. The results of the MP theory of light show that this assumption is not justified. We have also pointed out that the contribution of the atomic MDW to the total angular momentum of light is experimentally verifiable. In this work we have assumed a nondispersive medium, but the results can be straightforwardly generalized for dispersive media as done in the case of linear momentum in Ref. [35].

One interesting question that remains as a topic of further work is whether slow-light media could be used to amplify the MDW effect to allow its experimental verification in the same way as slow-light media have been used to amplify the rotary photon drag [77] and Fresnel drag effects [78]. This is, however, not obvious as the effects are fundamentally different. In the rotary photon drag and Fresnel drag experiments, light propagates through materials that are set in notable motion by external forces and the effects observed follow from this movement. In contrast, in the case of the MDW effect, the medium in which light propagates is initially at rest and the medium atoms become very slightly displaced by the optical force of the light field itself.

Very accurate technologies are presently becoming available for measuring the small atomic displacements on the surfaces of solid media. For example, the picometer-size atomic displacements of elastic waves generated at a highly reflective mirror interface have been a subject of a very recent careful study [79]. Therefore, we expect that by using a suitable setup, these technologies might also allow probing the atomic displacements generated by light while it is propagating inside the medium.

ACKNOWLEDGMENTS

This work has been funded in part by the Academy of Finland under Contracts No. 287074 and No. 318197 and the Aalto Energy Efficiency Research Programme. We also want to thank Tomaž Požar and Nelson G. C. Astrath for the recent communication, where we became aware of the paper of Poynting [61], the discussion of which has been added in the present work.

APPENDIX A: ANGULAR MOMENTUM SEPARATIONS

1. Spin and orbital angular momenta

In a nondispersive dielectric medium, the total angular momentum of the electromagnetic field in Eq. (1) can be written in terms of the vector potential $\mathbf{A}$ as [20,21,45,46]

$$\mathbf{J}_{\text{field}} = \varepsilon_0 \int E_i(\mathbf{r}\times\nabla)A_i d^3r + \varepsilon_0 \int \mathbf{E}\times\mathbf{A} d^3r - \varepsilon_0 \int (\mathbf{r}\times\mathbf{A})\mathbf{E}\cdot d\mathbf{S}, \tag{A1}$$

where ε_0 is the permittivity of vacuum. The vector potential $\mathbf{A}$ is related to the electric and magnetic fields by the conventional relations $\mathbf{E} = -\partial\mathbf{A}/\partial t$ and $\mathbf{B} = \nabla\times\mathbf{A}$ with $\mathbf{B} = \mu_0\mathbf{H}$, where μ_0 is the permeability of vacuum. In the first term on the right-hand side of Eq. (A1), we have used the Einstein summation convention.

For a light pulse, the fields approach zero at infinity. Therefore, the surface integral in the last term of Eq. (A1) will be zero, and we can identify the OAM and SAM terms as [20,21,80]

$$\mathbf{L}_{\text{field}} = \varepsilon_0 \int E_i(\mathbf{r}\times\nabla)A_i d^3r, \tag{A2}$$

$$\mathbf{S}_{\text{field}} = \varepsilon_0 \int \mathbf{E}\times\mathbf{A} d^3r. \tag{A3}$$

One can observe that these definitions of OAM and SAM in terms of the vector potential are in general gauge dependent. However, for fields that are exactly transverse, gauge invariance is obtained if $\mathbf{A}$ is defined to be the gauge invariant transverse vector potential [20,81].

The transverse field approximation is in many cases well justified. In the commonly used paraxial approximation of light beams, the electric and magnetic fields also have longitudinal components [65,82,83]. The magnitudes of these components are, however, typically negligible in comparison with the transverse field components. Therefore, in the paraxial approximation, Eqs. (A2) and (A3) can be used to separate the total angular momentum of light into the OAM and SAM parts reasonably accurately, but not exactly. In general, this separation is gauge dependent and only the total angular momentum of the electromagnetic field in Eq. (1) has a well-defined physical meaning. In this work we use the general definition of electromagnetic angular momentum in Eq. (1) in all our calculations. We also show that the movement of atoms in the MDW driven by the field carries a substantial part of the total angular momentum of light in a medium as described by Eq. (4).

2. External and internal angular momenta

In the case of a localized light pulse whose center of energy has a position vector $\mathbf{r}_0$, by a change of variables $\mathbf{r} \to \mathbf{r}_0 + \mathbf{r}'$, we can write Eq. (1) as

$$\mathbf{J}_{\text{field}} = \mathbf{J}_{\text{field,ext}} + \mathbf{J}_{\text{field,int}}, \tag{A4}$$

where $\mathbf{J}_{\text{field,ext}}$ and $\mathbf{J}_{\text{field,int}}$ are, respectively, the external and internal angular momenta of the field [44,50,51,53]. The external angular momentum is contributed by the OAM only, while the internal angular momentum is contributed by both the OAM and SAM. The origin-dependent external angular momentum is given by $\mathbf{J}_{\text{field,ext}} = \mathbf{r}_0 \times \mathbf{P}_{\text{field}}$, where $\mathbf{P}_{\text{field}} = \int \mathbf{g}_{\text{field}} d^3r$ is the total linear momentum of the electromagnetic field. Therefore, the definition of the external angular mo-

mentum corresponds to the classical definition of the angular momentum of a point particle. It gives zero if the angular momentum is calculated with respect to the propagation axis in which case $\mathbf{r}_0$ is parallel to $\mathbf{P}_{\text{field}}$. The internal angular momentum is given by $\mathbf{J}_{\text{field,int}} = \int \mathbf{r}' \times \mathbf{g}_{\text{field}} d^3r'$ and it does not depend on the choice of the origin. In the case of structured fields, the internal angular momentum $\mathbf{J}_{\text{field,int}}$ can be nonzero [19]. This is also shown in the simulation results. In the simulations we make the conventional choice that the origin lies in the optical axis so that the external angular momentum is zero. Therefore, we directly study the internal angular momentum quantities.

APPENDIX B: MONOCHROMATIC FIELD APPROXIMATION OF LIGHT PULSES

1. Linear polarization

In the monocromatic field limit with $\Delta k_0 \ll k_0$ we can approximate the k-dependent parts of the integrands in Eqs. (7) and (8) apart from the last part $u(k)e^{i[kz-\omega(k)t]}$ with the central frequency values as $\omega(k) \approx \omega_0$ and $k \approx k_{0,\text{med}} = nk_0$. After this, the integrals over k in Eqs. (7) and (8) can be evaluated analytically leading to the fields given by

$$\mathbf{E}_{p,l}(\mathbf{r},t) \approx \text{Re}\left[i\omega_0 \left(u_{p,l}\hat{\mathbf{x}} + \frac{i\partial u_{p,l}}{nk_0\partial x}\hat{\mathbf{z}} \right) e^{i(nk_0 z-\omega_0 t)} \right] \times e^{-(n\Delta k_0)^2(z-ct/n)^2/2}, \tag{B1}$$

$$\mathbf{H}_{p,l}(\mathbf{r},t) \approx \text{Re}\left[\frac{ink_0}{\mu_0} \left(u_{p,l}\hat{\mathbf{y}} + \frac{i\partial u_{p,l}}{nk_0\partial y}\hat{\mathbf{z}} \right) e^{i(nk_0 z-\omega_0 t)} \right] \times e^{-(n\Delta k_0)^2(z-ct/n)^2/2}. \tag{B2}$$

In the calculation of the optical force density by using Eq. (3), we need the Poynting vector. We perform part of our simulations by using the actual instantaneous Poynting vector and part of the simulations by using its time average over the harmonic cycle. As shown in Ref. [34], we can approximate the instantaneous Poynting vector of a light pulse with its time average over the harmonic cycle without losing accuracy in the calculation of the total linear and angular momenta, the transferred mass, and the averaged atomic displacements and velocities. This time-averaged Poynting vector is given by

$$\begin{aligned}
&\langle \mathbf{E}_{p,l}(\mathbf{r},t) \times \mathbf{H}_{p,l}(\mathbf{r},t) \rangle \\
&\approx \frac{n\omega_0^2}{2\mu_0 c}\text{Re}\left(\frac{iu_{p,l}\partial u^*_{p,l}}{nk_0\partial x}\hat{\mathbf{x}} - \frac{iu^*_{p,l}\partial u_{p,l}}{nk_0\partial y}\hat{\mathbf{y}} + |u_{p,l}|^2\hat{\mathbf{z}} \right) \\
&\quad \times e^{-(n\Delta k_0)^2(z-ct/n)^2} \\
&= -\frac{i\omega_0}{4\mu_0}(u^*_{p,l,k}\nabla u_{p,l,k} - u_{p,l,k}\nabla u^*_{p,l,k}) e^{-(n\Delta k_0)^2(z-ct/n)^2}.
\end{aligned} \tag{B3}$$

Here the first expression on the right is the explicit representation in the Cartesian basis and the second appealing expression is obtained by using $u_{p,l,k} = u_{p,l}e^{ink_0 z}$. For a LG beam without Gaussian form in the longitudinal direction, the corresponding result has been presented in the case of vacuum in Ref. [1].

2. Circular polarization

Using the same approximation as explained in the case of linear polarization above, the electric and magnetic fields of a right circularly polarized LG_{pl} pulse in Eqs. (9) and (10) can be written as

$$\begin{aligned}
\mathbf{E}_{p,l}(\mathbf{r},t) \approx \frac{1}{\sqrt{2}}\text{Re}\Bigg[&i\omega_0 \left(u_{p,l}\hat{\mathbf{x}} + \frac{i\partial u_{p,l}}{nk_0\partial x}\hat{\mathbf{z}} \right) e^{i(nk_0 z-\omega_0 t)} \\
&+ i\omega_0 \left(u_{p,l}\hat{\mathbf{y}} + \frac{i\partial u_{p,l}}{nk_0\partial y}\hat{\mathbf{z}} \right) e^{i(nk_0 z-\omega_0 t+\pi/2)} \Bigg] \\
&\times e^{-(n\Delta k_0)^2(z-ct/n)^2/2},
\end{aligned} \tag{B4}$$

$$\begin{aligned}
\mathbf{H}_{p,l}(\mathbf{r},t) \approx \frac{1}{\sqrt{2}}\text{Re}\Bigg[&\frac{ink_0}{\mu_0} \left(u_{p,l}\hat{\mathbf{y}} + \frac{i\partial u_{p,l}}{nk_0\partial y}\hat{\mathbf{z}} \right) e^{i(nk_0 z-\omega_0 t)} \\
&- \frac{ink_0}{\mu_0} \left(u_{p,l}\hat{\mathbf{x}} + \frac{i\partial u_{p,l}}{nk_0\partial x}\hat{\mathbf{z}} \right) e^{i(nk_0 z-\omega_0 t+\pi/2)} \Bigg] \\
&\times e^{-(n\Delta k_0)^2(z-ct/n)^2/2}.
\end{aligned} \tag{B5}$$

The Poynting vector time averaged over the harmonic cycle is then given by

$$\begin{aligned}
&\langle \mathbf{E}_{p,l}(\mathbf{r},t) \times \mathbf{H}_{p,l}(\mathbf{r},t) \rangle \\
&\approx \frac{n\omega_0^2}{2\mu_0 c}\text{Re}\left[\frac{u_{p,l}}{nk_0}\left(\frac{\partial u^*_{p,l}}{\partial y} + i\frac{\partial u^*_{p,l}}{\partial x} \right)\hat{\mathbf{x}} \right. \\
&\quad \left. - \frac{u^*_{p,l}}{nk_0}\left(\frac{\partial u_{p,l}}{\partial x} + i\frac{\partial u_{p,l}}{\partial y} \right)\hat{\mathbf{y}} + |u_{p,l}|^2\hat{\mathbf{z}} \right] \\
&\quad \times e^{-(n\Delta k_0)^2(z-ct/n)^2} \\
&= -\frac{i\omega_0}{4\mu_0}\left(u^*_{p,l,k}\nabla u_{p,l,k} - u_{p,l,k}\nabla u^*_{p,l,k} - i\frac{\partial |u_{p,l,k}|^2}{\partial r}\hat{\boldsymbol{\phi}} \right) \\
&\quad \times e^{-(n\Delta k_0)^2(z-ct/n)^2},
\end{aligned} \tag{B6}$$

where $\hat{\boldsymbol{\phi}} = -\sin(\phi)\hat{\mathbf{x}} + \cos(\phi)\hat{\mathbf{y}}$ is the azimuthal unit vector. Again, the first expression on the right is the explicit representation in the Cartesian basis and the second appealing expression is obtained by using $u_{p,l,k} = u_{p,l}e^{ink_0 z}$. In the last expression, the first two terms inside the parentheses are polarization independent and relate to the OAM while the last term is polarization dependent and relates to the SAM. For a LG beam without Gaussian form in the longitudinal direction, the corresponding result has been presented in the case of vacuum in Ref. [1].

[1] L. Allen, M. W. Beijersbergen, R. J. C. Spreeuw, and J. P. Woerdman, Orbital angular momentum of light and the transformation of Laguerre-Gaussian laser modes, Phys. Rev. A **45**, 8185 (1992).

[2] A. Mair, A. Vaziri, G. Weihs, and A. Zeilinger, Entanglement of the orbital angular momentum states of photons, Nature (London) **412**, 313 (2001).

[3] D. G. Grier, A revolution in optical manipulation, Nature (London) **424**, 810 (2003).

[4] R. C. Devlin, A. Ambrosio, N. A. Rubin, J. P. B. Mueller, and F. Capasso, Arbitrary spin-to-orbital angular momentum conversion of light, Science **358**, 896 (2017).

[5] N. Bozinovic, Y. Yue, Y. Ren, M. Tur, P. Kristensen, H. Huang, A. E. Willner, and S. Ramachandran, Terabit-scale orbital angular momentum mode division multiplexing in fibers, Science **340**, 1545 (2013).

[6] Z. Shao, J. Zhu, Y. Chen, Y. Zhang, and S. Yu, Spin-orbit interaction of light induced by transverse spin angular momentum engineering, Nat. Commun. **9**, 926 (2018).

[7] T. Satoh, R. Iida, T. Higuchi, Y. Fujii, A. Koreeda, H. Ueda, T. Shimura, K. Kuroda, V. I. Butrim, and B. A. Ivanov, Excitation of coupled spin-orbit dynamics in cobalt oxide by femtosecond laser pulses, Nat. Commun. **8**, 638 (2017).

[8] L. Du, Z. Man, Y. Zhang, C. Min, S. Zhu, and X. Yuan, Manipulating orbital angular momentum of light with tailored in-plane polarization states, Sci. Rep. **7**, 41001 (2017).

[9] G. Molina-Terriza, J. P. Torres, and L. Torner, Twisted photons, Nat. Photon. **3**, 305 (2007).

[10] G. Gibson, J. Courtial, M. J. Padgett, M. Vasnetsov, V. Pas'ko, S. M. Barnett, and S. Franke-Arnold, Free-space information transfer using light beams carrying orbital angular momentum, Opt. Express **12**, 5448 (2004).

[11] H. He, M. E. J. Friese, N. R. Heckenberg, and H. Rubinsztein-Dunlop, Direct Observation of Transfer of Angular Momentum to Absorptive Particles from a Laser Beam with a Phase Singularity, Phys. Rev. Lett. **75**, 826 (1995).

[12] M. E. J. Friese, T. A. Nieminen, N. R. Heckenberg, and H. Rubinsztein-Dunlop, Optical alignment and spinning of laser-trapped microscopic particles, Nature (London) **394**, 348 (1998).

[13] A. T. O'Neil, I. MacVicar, L. Allen, and M. J. Padgett, Intrinsic and Extrinsic Nature of the Orbital Angular Momentum of a Light Beam, Phys. Rev. Lett. **88**, 053601 (2002).

[14] V. Garcés-Chávez, D. McGloin, M. J. Padgett, W. Dultz, H. Schmitzer, and K. Dholakia, Observation of the Transfer of the Local Angular Momentum Density of a Multiringed Light Beam to an Optically Trapped Particle, Phys. Rev. Lett. **91**, 093602 (2003).

[15] M. Beijersbergen, R. Coerwinkel, M. Kristensen, and J. Woerdman, Helical-wavefront laser beams produced with a spiral phaseplate, Opt. Commun. **112**, 321 (1994).

[16] K. Sueda, G. Miyaji, N. Miyanaga, and M. Nakatsuka, Laguerre-Gaussian beam generated with a multilevel spiral phase plate for high intensity laser pulses, Opt. Express **12**, 3548 (2004).

[17] V. V. Kotlyar, A. A. Almazov, S. N. Khonina, V. A. Soifer, H. Elfstrom, and J. Turunen, Generation of phase singularity through diffracting a plane or gaussian beam by a spiral phase plate, J. Opt. Soc. Am. A **22**, 849 (2005).

[18] B. Terhalle, A. Langner, B. Päivänranta, V. A. Guzenko, C. David, and Y. Ekinci, Generation of extreme ultraviolet vortex beams using computer generated holograms, Opt. Lett. **36**, 4143 (2011).

[19] A. M. Yao and M. J. Padgett, Orbital angular momentum: Origins, behavior and applications, Adv. Opt. Photon. **3**, 161 (2011).

[20] B. Piccirillo, S. Slussarenko, L. Marrucci, and E. Santamato, The orbital angular momentum of light: Genesis and evolution of the concept and of the associated photonic technology, Riv. Nuovo Cimento **36**, 501 (2013).

[21] D. L. Andrews and M. Babiker, *The Angular Momentum of Light* (Cambridge University Press, Cambridge, 2013).

[22] K. Y. Bliokh, F. J. Rodríguez-Fortuño, F. Nori, and A. V. Zayats, Spin-orbit interactions of light, Nat. Photon. **9**, 796 (2015).

[23] F. Alpeggiani, K. Y. Bliokh, F. Nori, and L. Kuipers, Electromagnetic Helicity in Complex Media, Phys. Rev. Lett. **120**, 243605 (2018).

[24] J. Lin, J. P. B. Mueller, Q. Wang, G. Yuan, N. Antoniou, X.-C. Yuan, and F. Capasso, Polarization-controlled tunable directional coupling of surface plasmon polaritons, Science **340**, 331 (2013).

[25] K. Y. Bliokh, A. Y. Bekshaev, and F. Nori, Optical Momentum, Spin, and Angular Momentum in Dispersive Media, Phys. Rev. Lett. **119**, 073901 (2017).

[26] K. Y. Bliokh, A. Y. Bekshaev, and F. Nori, Extraordinary momentum and spin in evanescent waves, Nat. Commun. **5**, 3300 (2014).

[27] X.-G. Luo, M.-B. Pu, X. Li, and X.-L. Ma, Broadband spin hall effect of light in single nanoapertures, Light Sci. Appl. **6**, e16276 (2017).

[28] R. Bhandari, Polarization of light and topological phases, Phys. Rep. **281**, 1 (1997).

[29] Z. Bomzon, G. Biener, V. Kleiner, and E. Hasman, Space-variant Pancharatnam–Berry phase optical elements with computer-generated subwavelength gratings, Opt. Lett. **27**, 1141 (2002).

[30] K. Y. Bliokh, A. Niv, V. Kleiner, and E. Hasman, Geometrodynamics of spinning light, Nat. Photon. **2**, 748 (2008).

[31] K. Y. Bliokh, Y. Gorodetski, V. Kleiner, and E. Hasman, Coriolis Effect in Optics: Unified Geometric Phase and Spin-Hall Effect, Phys. Rev. Lett. **101**, 030404 (2008).

[32] X. Ling, X. Zhou, K. Huang, Y. Liu, C.-W. Qiu, H. Luo, and S. Wen, Recent advances in the spin Hall effect of light, Rep. Prog. Phys. **80**, 066401 (2017).

[33] X. Ling, X. Zhou, X. Yi, W. Shu, Y. Liu, S. Chen, H. Luo, S. Wen, and D. Fan, Giant photonic spin Hall effect in momentum space in a structured metamaterial with spatially varying birefringence, Light Sci. Appl. **4**, e290 (2015).

[34] M. Partanen, T. Häyrynen, J. Oksanen, and J. Tulkki, Photon mass drag and the momentum of light in a medium, Phys. Rev. A **95**, 063850 (2017).

[35] M. Partanen and J. Tulkki, Mass-polariton theory of light in dispersive media, Phys. Rev. A **96**, 063834 (2017).

[36] M. E. J. Friese, J. Enger, H. Rubinsztein-Dunlop, and N. R. Heckenberg, Optical angular-momentum transfer to trapped absorbing particles, Phys. Rev. A **54**, 1593 (1996).

[37] N. B. Simpson, K. Dholakia, L. Allen, and M. J. Padgett, Mechanical equivalence of spin and orbital angular momentum of light: An optical spanner, Opt. Lett. **22**, 52 (1997).

[38] H. Adachi, S. Akahoshi, and K. Miyakawa, Orbital motion of spherical microparticles trapped in diffraction patterns of circularly polarized light, Phys. Rev. A **75**, 063409 (2007).

[39] J. D. Jackson, *Classical Electrodynamics* (Wiley, New York, 1999).

[40] L. D. Landau, E. M. Lifshitz, and L. P. Pitaevskii, *Electrodynamics of Continuous Media* (Pergamon, Oxford, 1984).

[41] L. D. Landau and E. M. Lifshitz, *The Classical Theory of Fields* (Pergamon, Oxford, 1989).

[42] E. Leader and C. Lorcé, The angular momentum controversy: What's it all about and does it matter? Phys. Rep. **541**, 163 (2014).

[43] M. V. Berry, Optical currents, J. Opt. A **11**, 094001 (2009).

[44] D. Lenstra and L. Mandel, Angular momentum of the quantized electromagnetic field with periodic boundary conditions, Phys. Rev. A **26**, 3428 (1982).

[45] S. van Enk and G. Nienhuis, Eigenfunction description of laser beams and orbital angular momentum of light, Opt. Commun. **94**, 147 (1992).

[46] S. J. van Enk and G. Nienhuis, Spin and orbital angular momentum of photons, Europhys. Lett. **25**, 497 (1994).

[47] G. Nienhuis and L. Allen, Paraxial wave optics and harmonic oscillators, Phys. Rev. A **48**, 656 (1993).

[48] S. M. Barnett and L. Allen, Orbital angular momentum and nonparaxial light beams, Opt. Commun. **110**, 670 (1994).

[49] S. M. Barnett, Optical angular-momentum flux, J. Opt. B **4**, S7 (2002).

[50] R. Jáuregui and S. Hacyan, Quantum-mechanical properties of Bessel beams, Phys. Rev. A **71**, 033411 (2005).

[51] G. F. Calvo, A. Picón, and E. Bagan, Quantum field theory of photons with orbital angular momentum, Phys. Rev. A **73**, 013805 (2006).

[52] S. Hacyan and R. Jáuregui, A relativistic study of Bessel beams, J. Phys. B **39**, 1669 (2006).

[53] C.-F. Li, Spin and orbital angular momentum of a class of nonparaxial light beams having a globally defined polarization, Phys. Rev. A **80**, 063814 (2009).

[54] A. Aiello, N. Lindlein, C. Marquardt, and G. Leuchs, Transverse Angular Momentum and Geometric Spin Hall Effect of Light, Phys. Rev. Lett. **103**, 100401 (2009).

[55] A. Aiello, C. Marquardt, and G. Leuchs, Transverse angular momentum of photons, Phys. Rev. A **81**, 053838 (2010).

[56] I. Bialynicki-Birula and Z. Bialynicka-Birula, Canonical separation of angular momentum of light into its orbital and spin parts, J. Opt. **13**, 064014 (2011).

[57] S. M. Barnett, Rotation of electromagnetic fields and the nature of optical angular momentum, J. Mod. Opt. **57**, 1339 (2010).

[58] A. M. Stewart, Comparison of different forms for the "spin" and "orbital" components of the angular momentum of light, Int. J. Opt. **2011**, 728350 (2011).

[59] R. P. Cameron, F. C. Speirits, C. R. Gilson, L. Allen, and S. M. Barnett, The azimuthal component of Poynting's vector and the angular momentum of light, J. Opt. **17**, 125610 (2015).

[60] T. G. Philbin and O. Allanson, Optical angular momentum in dispersive media, Phys. Rev. A **86**, 055802 (2012).

[61] J. H. Poynting, On small longitudinal material waves accompanying light waves, Proc. R. Soc. Lond. A **85**, 474 (1911).

[62] C. Kittel, *Introduction to Solid State Physics* (Wiley, Hoboken, NJ, 2005).

[63] P. W. Milonni and R. W. Boyd, Momentum of light in a dielectric medium, Adv. Opt. Photon. **2**, 519 (2010).

[64] A. Cerjan and C. Cerjan, Orbital angular momentum of Laguerre-Gaussian beams beyond the paraxial approximation, J. Opt. Soc. Am. A **28**, 2253 (2011).

[65] L. Allen and M. Padgett, The orbital angular momentum of light: An introduction, in *Twisted Photons: Applications of Light with Orbital Angular Momentum*, edited by J. P. Torres and L. Torner (Wiley, Weinheim, 2011), pp. 1–12.

[66] H. A. Haus, *Waves and Fields in Optoelectronics* (Prentice-Hall, Englewood Cliffs, NJ, 1984).

[67] I. R. Kenyon, *The Light Fantastic* (Oxford University Press, Oxford, 2008).

[68] H. H. Li, Refractive index of silicon and germanium and its wavelength and temperature derivatives, J. Phys. Chem. Ref. Data **9**, 561 (1980).

[69] D. R. Lide, Ed., *CRC Handbook of Chemistry and Physics* (CRC, Boca Raton, FL, 2004).

[70] M. A. Hopcroft, W. D. Nix, and T. W. Kenny, What is the Young's modulus of silicon? J. Microelectromech. Syst. **19**, 229 (2010).

[71] See Supplemental Material at http://link.aps.org/supplemental/10.1103/PhysRevA.98.033813 for video files of the simulated atomic displacements and velocities of linearly and circularly polarized Laguerre-Gaussian pulses.

[72] A. Ashkin, J. M. Dziedzic, J. E. Bjorkholm, and S. Chu, Observation of a single-beam gradient force optical trap for dielectric particles, Opt. Lett. **11**, 288 (1986).

[73] M. Partanen and J. Tulkki, Light-driven mass density wave dynamics in optical fibers, Opt. Express **26**, 22046 (2018).

[74] C. Schinke, P. C. Peest, J. Schmidt, R. Brendel, K. Bothe, M. R. Vogt, I. Kröger, S. Winter, A. Schirmacher, S. Lim, H. T. Nguyen, and D. MacDonald, Uncertainty analysis for the coefficient of band-to-band absorption of crystalline silicon, AIP Adv. **5**, 067168 (2015).

[75] M. A. Green, Self-consistent optical parameters of intrinsic silicon at 300 K including temperature coefficients, Sol. Energy Mater. Sol. Cells **92**, 1305 (2008).

[76] B. Cowan, Optical damage threshold of silicon for ultrafast infrared pulses, AIP Conf. Proc. **877**, 837 (2006).

[77] S. Franke-Arnold, G. Gibson, R. W. Boyd, and M. J. Padgett, Rotary photon drag enhanced by a slow-light medium, Science **333**, 65 (2011).

[78] A. Safari, I. De Leon, M. Mirhosseini, O. S. Magaña Loaiza, and R. W. Boyd, Light-Drag Enhancement by a Highly Dispersive Rubidium Vapor, Phys. Rev. Lett. **116**, 013601 (2016).

[79] T. Požar, J. Laloš, A. Babnik, R. Petkovšek, M. Bethune-Waddell, K. J. Chau, G. V. B. Lukasievicz, and N. G. C. Astrath, Isolated detection of elastic waves driven by the momentum of light, Nat. Commun. **9**, 3340 (2018).

[80] T. A. Nieminen, A. B. Stilgoe, N. R. Heckenberg, and H. Rubinsztein-Dunlop, Angular momentum of a strongly focused Gaussian beam, J. Opt. A **10**, 115005 (2008).

[81] C. Cohen-Tannoudji, J. Dupont-Roc, and G. Grynberg, *Photons and Atoms: Introduction to Quantum Electrodynamics* (Wiley, New York, 1989).

[82] A. Carnicer, I. Juvells, D. Maluenda, R. Martínez-Herrero, and P. M. Mejías, On the longitudinal component of paraxial fields, Eur. J. Phys. **33**, 1235 (2012).

[83] M. Lax, W. H. Louisell, and W. B. McKnight, From Maxwell to paraxial wave optics, Phys. Rev. A **11**, 1365 (1975).